Proceedings World Geothermal Congress 2015
Melbourne, Australia, 19-25 April 2015

Moment Partitioning for Injection-Induced Seismicity: Case Studies & Insights from Numerical Modeling

L. Buijze, B. Wassing, P.A. Fokker, and J.D. van Wees

TNO (Dutch Geological Survey), Princetonlaan 6, 3584CB, Utrecht, The Netherlands

loes.buijze@tno.nl

Keywords: EGS, induced seismicity, moment partioning, coupled hydro-mechanical model, seismogenic index

ABSTRACT

In order to understand and mitigate felt seismicity induced by fluid injection activities such as Enhanced Geothermal Systems, it is important to know what controls the seismic response to the injection of a certain volume. A recent study proposed an upper bound to induced magnitudes that can be expected based on injected volume and shear modulus. However, this upper bound is mostly not released during injection. The physical controls on the measure of the seismic moment release with respect to this theoretical maximum are yet unknown. In this study we investigate the moment partitioning (the ratio of observed moment to the predicted moment which is a function of volume and shear modulus) of injection sites worldwide and compare it against various site specific and injection parameters. In addition, for a select number of sites we track the moment partitioning as a function of injection time. With a coupled hydro-mechanical model we model the seismic response for a generic injection case and are able to reproduce some of the trends observed in the case studies.

1 INTRODUCTION

Geothermal energy is an important renewable energy form with a large potential. One form of geothermal energy is an Enhanced Geothermal System, which exploits hot, relatively impermeable rock, often at great depth to produce steam to generate electricity (Majer et al., 2007). To increase the permeability, the pre-existing fracture network in the impermeable rock mass needs to be stimulated by the injection of water at high pressures. The increase in pore pressure leads to reactivation of the fractures in tensile and shear failure, which enhances the permeability. Shear on fractures and faults can occur seismically, producing seismic events which are monitored closely during injection experiments. The majority of event magnitudes observed were very small (M<1), but several larger events (M>2.5) which can be felt at the surface have occurred as a result of the stimulations, and caused great concern amonst the local population. The best known example is the M_L 3.4 earthquake near Basel (Häring et al., 2008), which led to the termination of the EGS project. Also, the M_L 2.9 which occurred at Soultz-sous-Forêts led to the suspension of the project. This emphasizes the need to understand what key factors and mechanisms influence the occurrence of larger magnitudes, so that mitigation measures may be taken in the future.

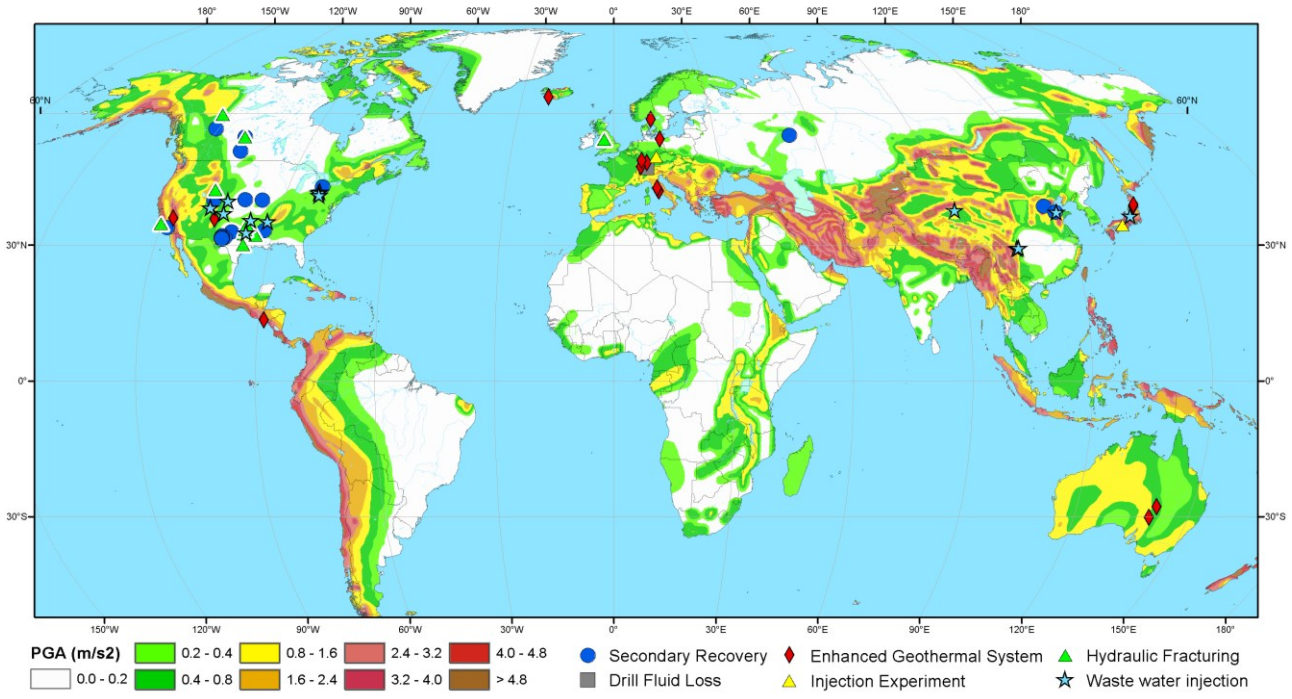

Figure 1 Reported occurrences of injection-induced seismicity worldwide. The background colors indicate the natural seismic hazard, given in Peak Ground Acceleration (PGA, ms^{-2}) with a 10% probability of exceedance in 50 years (Giardini et al., 1999) .

Several studies identified key parameters influencing the induced event magnitudes in EGS. From individual injection experiments it was observed that event number and size respond to varying injection rates (Cuenot et al., 2008). The focal mechanisms of the seismic events indicated that the (larger) events took place on larger fault structures which are often oriented favorably in the stress field (eg. Deichmann & Ernst, 2009; Fehler, 1989; Moeck et al., 2009). An important aspect is the occurrence seismicity after shut-in of the well, due to the ongoing diffusion of pore pressure in the rock mass even. A number of the largest events in relationship with EGS actually took place in the post-injection period, such as the Berlín M_L 4.4 (Bommer et al., 2006), the Basel M_L 3.4 (Häring et al., 2008), the Soultz-sous-Forêts M_L 2.3 in 2000 and M_L 2.9 in 2003 (Charléty et al., 2007). These events often occur at the fringes of the seismic cloud, where pore pressures are still increasing due to diffusion. An investigation of the seismicity in 41 EGS in Europe suggests crystalline rock to be more prone to seismicity than do sedimentary rock (Evans et al., 2012). Broader studies investigating not only seismicity in EGS but also seismicity occurring in other types of induced seismicity show that maximum magnitudes increase with the length scale of the activity (McGarr, 2002; S. Shapiro et al., 2011), mass change (Klose, 2013) or volume change (McGarr, 2014; Nicol et al., 2011). An upper bound of magnitudes was proposed as a function of volume change and shear modulus (McGarr, 2014). An overview of worldwide occurrences of injection induced seismicity is shown in Figure 1. There is however a large amount of scatter in the data; some injections yield relatively low magnitudes or no seismicity at all, others yield events close to the upper bound proposed for the injection volume. This is also indicated by the large differences in seismogenic index, which denotes the seismotectonic state of an injection reservoir (i.e. to what measure it responds to the injection) (Dinske & Shapiro, 2013; S. A. Shapiro et al., 2010). It is yet unclear what physical properties and processes influences this seismic response.

In this research we have further evaluated the seismic response to a certain injected volume, and its dependency on physical processes. The first part of the research focuses on the seismic response and the maximum magnitudes of injection cases worldwide, including observations from hydraulic fracturing, waste water injection, secondary recovery, and other types of injections. Also we investigate the seismic response as a function of time during injection for a number of cases where enough data is available. The second part of our research focuses on numerical modeling of injection induced seismicity using a coupled hydro-mechanical model. The evolution of the seismic response with time obtained from the model results will be compared to the observations from cases presented in the first part of the study. Implications for Enhanced Geothermal Systems will be discussed.

2 DATA & ANALYSES

The dataset for this study was composed of data reported in the literature on (Enhanced) Geothermal Systems, hydraulic fracturing, waste water injections, secondary recovery and scientific water injection experiments during which seismic events occurred. Individual injection experiments at the same site were treated as separate data. For injection experiments we collect the following parameters for our analyses:

- Maximum magnitude M_{max} (M_w): The maximum magnitude recorded in relationship to the operation. Where possible we converted the magnitude to moment magnitude M_w. To convert M_{max} to seismic moment, we used the scaling relationship proposed by (Hanks & Kanamori, 1979).
- Depth of the event d_{mmax} (m): The depth of the hypocenter of the M_{max} event, where reported. Where reported, uncertainties are 800 m or less for the studied events, except the event in the Rongchang water injection where the uncertainty in depth is 5 km.
- Operational parameters: Volume change ΔV (m^3) which is the fluid injected at the moment M_{max} occurred, the average injection pressure ΔP.
- Depth d (m) and): Depth of the injection. If the injection took place over an interval, the average depth was taken.
- Rocktype
- Peak Ground Acceleration (PGA) (ms^{-2}) as a proxy for the regional seismic activity, taken from the Global Seismic Hazard map (Giardini et al., 1999).

The parameters are summarized in the table at the end of the document.

2.1 Volume change and seismic moment

The injection of a fluid volume in the subsurface raises the pore pressure and strains the rock mass. This strain energy creates shear on pre-existing faults and fractures, stresses which can be released through (seismic) motion. A formula relating the injected volume ΔV to the cumulative seismic moment ΣM_0 was given by McGarr (2014)

$$\sum M_0 = 2G\Delta V \tag{1}$$

where G is the shear modulus (Pa). For a typical frequency-magnitude distribution with a slope of 1, the seismic moment of the maximum magnitude M_{max} is ½ of the cumulative seismic moment ΣM_0, reducing equation (1) to

$$M_0 = G\Delta V \tag{2}$$

In this study we used equation (2) to estimate the theoretical moment resulting from the injected volume at the moment of M_{max}. We compared this theoretical moment to the observed moment, and quantified the ratio between the observed moment and the theoretical moment with the *moment fraction or moment partitioning* θ. Seismicity is not only a function of the strain energy change due to the activity, but also of the pre-existing strain energy. In formula (1) it was assumed faults in the fluid-affected

volume are ½ a stress drop away from failure, and hence the pre-existing state was partly taken into account, i.e. faults are halfway in their loading cycle. In this study we did not make a distinction between induced and triggered, because the boundary between the two is not a sharp one. We can however speak of 'tectonic dominated' or 'perturbation dominated' events when comparing the moment fractions.

The shear modulus is often not reported, we use average values corresponding to the rock type into which the fluid was injected. For granites and other igneous rocks we used a shear modulus of 24 GPa, for limestones & dolomites 22 GPa., for sandstones 15 GPa and for shales 15 GPa. In case the rocktype was unknown, we used an average value of 20 GPa.

2.2 Seismicity and moment fraction as a function of injection time

For a number of cases we investigate the evolution of seismicity and the moment fraction θ during injection (Table 1). In these cases we compute the cumulative seismic moment ΣM_0 and use equation (1) to estimate the theoretical cumulative seismic moment. Also during these experiments we assume a constant b-value of 1.

Table 1 Summary of cases where the seismic moment release as investigated as a function of injection volume ΔV (m^3) throughout the injection period. EGS=Enhanced Geothermal System, HF= hydraulic fracturing, EXP = Fluid injection experiment, WWI = waste water injection. Seismic moment M_0 is the total seismic moment release during the injection period, given in Nm.

Site	Type	Start	Duration	Total ΔV	Total M_0	Rocktype	Reference
Soultz-sous-Forets GPK3 phase 1 (FRA)	EGS	27-5-2003	5.7 days	3.90E+04	1.75E+14	Granite	(Cuenot et al., 2008; Dorbath et al., 2009)
Basel Main stimulation (CHE)	EGS	2-12-2006	6 days	1.15E+04	3.50E+13	Granite	(Häring et al., 2008)
Paralana (AUS)	EGS	10-7-2010	4.5 days	1.65E+05	2.23E+15	Granite	(Bendall et al., 2014)
Barnett Shale (USA)	HF	--	80 min	5.19E+02	1.21E+06	Shale	(Maxwell et al., 2008)
KTB 1994 Stimulation (DEU)	EXP	17-12-1994	26 hours	2.34E+02	8.98E+10	Gneiss	(Jost et al., 1998)
Rocky Mountain Arsenal 1st injection (USA)	WWI	1-3-1962	7 months	3.81E+05	1.25E+15	Crystalline	(Healy et al., 1966)
Cotton Valley B	HF	1997.00	3.2 hours	1.25E+03	2.50E+9	Sands & Shales	(Rutledge et al., 2004)
Cotton Valley E	HF	1997.00	4.5 hours	4.00E+02	4.43E+10	Sands & Shales	(Rutledge et al., 2004)

2.3 Block-Spring model of fluid injection into a fault

To further investigate the controlling parameters of the observed seismicity and moment fraction as a function of injection time, we modeled a generic injection case using the Block-Spring model presented in Wassing et al. (in press), which was based on the block-spring model of (Baisch et al., 2010). The Block-Spring model simulates coupled flow and mechanics on a single 2-D fault plane surface of 4000 x 4000 m, divided in grid cells of 20 m (Figure 2). The fracture plane dips 60° in the direction of the minimum horizontal stress S_h to a maximum depth of 6500 m. The vertical stress was computed assuming an average overburden density of 2550 kgm^{-3}, pore pressure as hydrostatic and the minimum and maximum horizontal stresses were equal and were both $0.6*S_v$, which implies a state of stress at or near the failure equilibrium for a friction coefficient μ of 0.6. An injection well was situated in the middle of the fault plane at a depth of 4750 m, injecting water at an imposed flow rate. For this generic case, water was injected at a constant flow rate of 75.6 l/s. It was assumed flow only takes place within the fault plane. The fault cells had an initial permeability of 6 mD, which could be increased due to shear slip to a maximum of 750 mD. Transient pressure at the injection point and pore pressure p in the grid cells was computed using a Runge Kutta solver. The increase of pressure decreases the normal stress σ_n on the fault cells, which are governed by the Mohr-Coulomb friction criterion

$$\tau = C + (\sigma_n - p)\mu \tag{3}$$

where τ is the shear stress, C is the cohesion, and μ is the friction coefficient. Once the pressure buildup in a cell was large enough so that the failure criterion was reached, the flow simulation was halted and the cell entered the failure mode. This failure was simulated by prescribing a fixed stress drop $\Delta\sigma$ (MPa) to the cell. Subsequently 90% of this stress drop is be transferred to the neighbouring patches to simulate stress transfer (Figure 2b). This is an approximation of the rupture and stress transfer physics, but to a first order reproduces similar trends as does hydro-mechanical software based on more realistic failure and stress transfer physics (Wassing et al., in press). The stress transfer can cause neighboring patches to fail also if their failure criterion is exceeded, which may again trigger further patches, creating an avalanche resulting in a large slip event. The seismic moment M_0 (Nm) can be computed from the slipped area S (m^2), that can be obtained from the model, and the prescribed stress drop $\Delta\sigma$ (MPa) using the following formula for stress drop on a circular fault (Eshelby, 1957)

$$M_0 = \left(\frac{S}{\pi}\right)^{\frac{3}{2}} \frac{16}{7}\Delta\sigma \tag{4}$$

The shear slip on the patches increased the permeability, which we approximated through an increase of permeability with a constant factor per slip event. After the patches no longer slip, the flow simulation is resumed using the updated permeability and continues until the next slip event takes place.

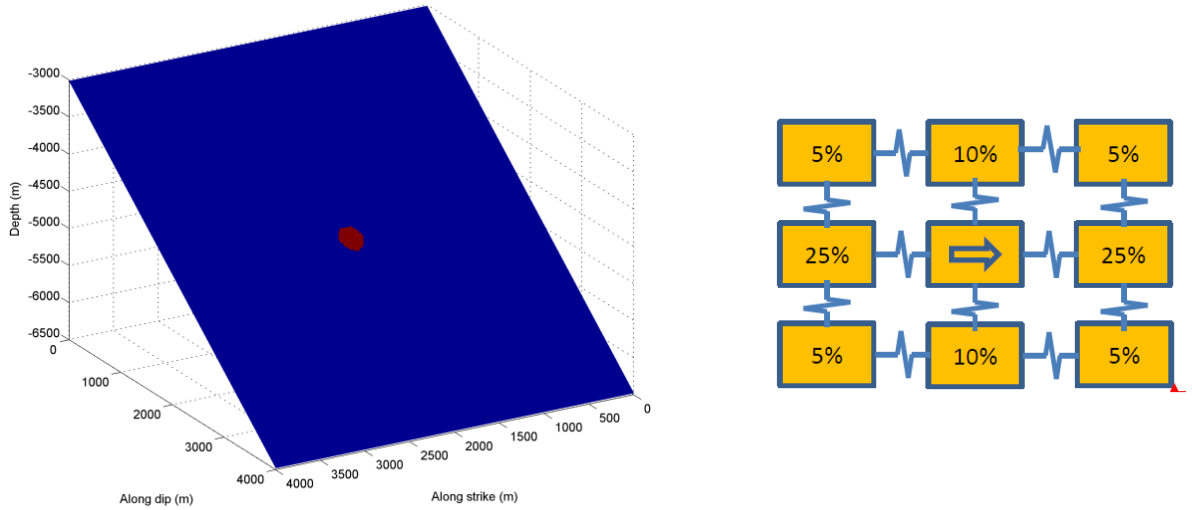

Figure 2 a) Model geometry showing single fault plane dipping 60° in the direction of S_h. The injection well is located in the middle (red dot) b) Prescription of stress transfer to neighboring fault patches. In total 90% of the stress drop of the failed patch is transferred.

3 SEISMIC MOMENT PARTIONING OBSERVED FOR INJECTION EXPERIMENTS

3.1 Seismic moment & injected volume

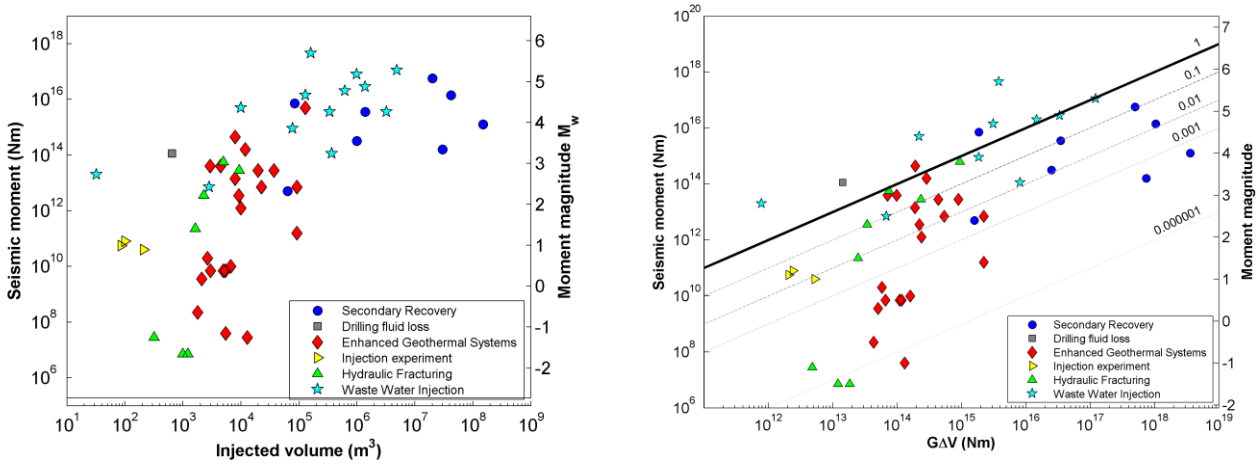

Figure 3 a) Injected volume against maximum magnitude for injection induced seismicity

Reported seismic magnitudes seem to increase with the injected volumes ΔV though the scatter is large (Figure 3). Each activity has its own characteristic range of injected volumes and induced magnitudes. During hydraulic fracturing the smallest volumes, usually 100's – 1000's of m^3, are injected during a single fracture stage, although the massive injections in the Horn River Basin may range up to 10,000 m^3 per fracture stage. The largest event that occurred during hydraulic fracturing is a M_L 3.8 in the Horn River Basin. In Enhanced Geothermal Systems the rock is stimulated typically with 1,000 – 100,000 m^3 of fluid, with observed magnitudes ranging up to M 4.4 in Berlín, El Salvador. The largest events with M>5 were associated with waste water injection and secondary recovery, where volumes of up to respectively 10^7 and 10^8 m^3 have been injected.

Another important observation is that the absolute volume sufficient enough to induce seismic events with M >2 appears to be quite small. The most extreme example is the injection at Matsushiro, Japan, where the injection of 32.4 m^3 was associated with a M 2.8 event (Ohtake, 1974). The water seemed to have flowed directly into the Matsushiro fault zone, traveling for a distance of ~3 km before triggering a small earthquake swarm. A more recent example is the event induced during drilling of a geothermal well in Saint Gallen, Switzerland, where drilling mud losses of 650 m^3 induced a M_L 3.5. Again fluid appeared to have migrated in a large fault zone, which had been identified on seismics but was thus far inactive. The amount of volume injected versus the seismic

output was further evaluated by comparing the theoretical seismic moments computed using equation 2 against the maximum seismic moments recorded (Figure 3b). Though most of the moments fractions (dashed lines) are very small, some fractions actually exceed 1, indicating the the seismic moment is much larger than the theoretical moment needed to accommodate the injected volume. A moment fraction >1 was observed for several waste water injection sites; at Matsushiro, Prague (OK), Huajiachang gas field and the Rocky Mountain Arsenal. Also a moment fraction >1 was observed for Saint Gallen and secondary recovery in the Renqiu oil field.

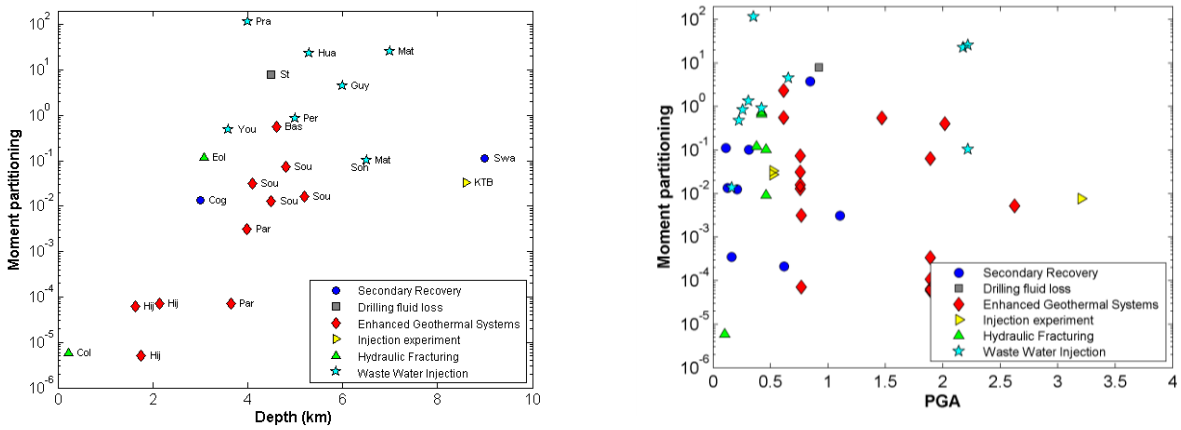

Figure 4 a) Moment partitioning versus hypocenter depth of M_{max}. b) Moment partitioning as a function of the regional seismic hazard expressed in Peak Ground Acceleration (PGA, ms^{-2}) with a 10% probability of exceedance in 50 years.

We investigate the moment partitioning against a number of parameters. Moment fractions >1 are observed only for mainshocks which occurred at depths greater than 4 km (Figure 4a). Note that the activity itself may be much more shallow than the hypocenter depth. Fluids may migrate through permeable fault zones and trigger events at a deeper level. The natural seismic hazard does not seem of influence on the moment partitioning (Figure 4b).

3.2 Moment fraction as a function of injection

The seismic moment increases proportionally with the injected volume for most of the cases studied (Figure 5). The data often follow a path of constant moment partitioning, along the dashed lines. This is also evident in Figure 5b, where the moment fraction is plotted as a function of relative injection time. In some cases the moment fraction increases rapidly in the initial phases of the injection, such as for the Rocky Mountain Arsenal and Soultz-sous-Forêts. After some time (~10 – 20 % of the total injection time) the moment fraction becomes relatively constant. Moment fraction mostly vary between 10^{-4} and 10^{-1}, Occasionally the moment partitioning suddenly increases during the injection due to the occurrence of a relatively large events, such as is evident from the sudden jump in moment fraction in Figure 5b for the KTB94 and Rocky Mountain Arsenal injections.

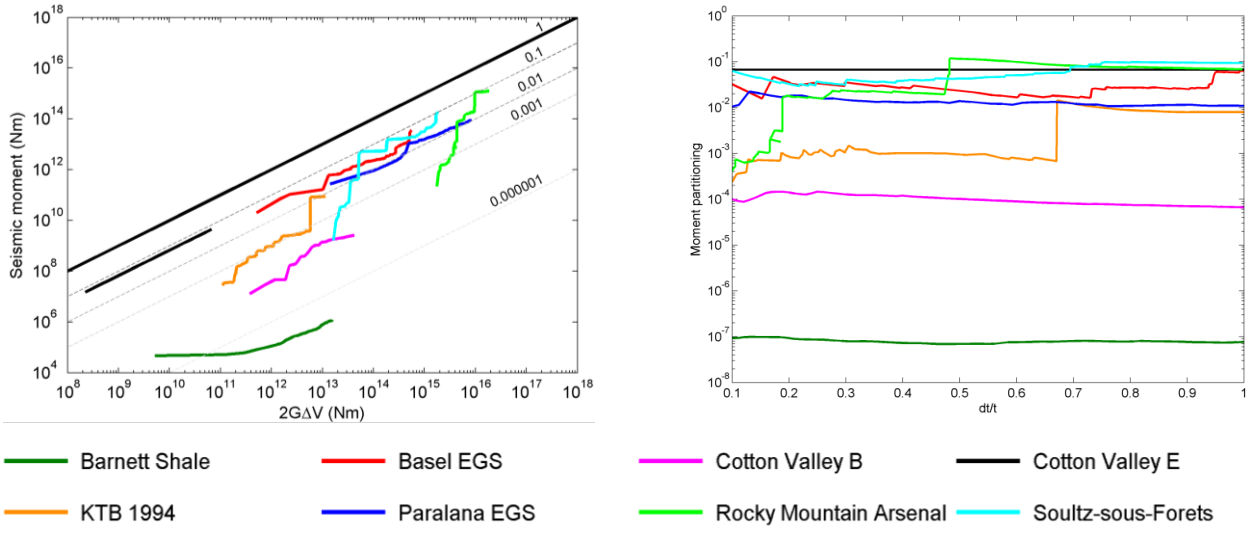

Figure 5 a) Evolution of the observed cumulative seismic moment with the volumetric moment as defined by equation (1). The data encompass events occurring during the injection experiment only, post-injection seismicity is not included in the plot. The bold line indicates where the cumulative seismic moment equals 2GΔV, a moment fraction of 1, and the dashed line indicate smaller moment fractions indicated by the numbers. b) the moment fraction of the same data as a function of relative injection time.

4 NUMERICAL MODELING OF THE EVOLUTION OF SEISMIC MOMENT WITH INJECTION

For the reference scenario we imposed a constant flow rate of 75.6 l/s at the injection point in the middle of the fault, with flow and friction properties as described in section 2.3. The failure surface and the pressure distribution after 70 hours of injection are shown in Figure 4a and b. The pressure front reaches a few 100 m's from the injection well. Slip events are confined to the zone of pressure increase and gradually reach a larger distance from the well, of up to 550 m at the end of the injection (Figure 6c). Events keep taking place near the injection point as well.

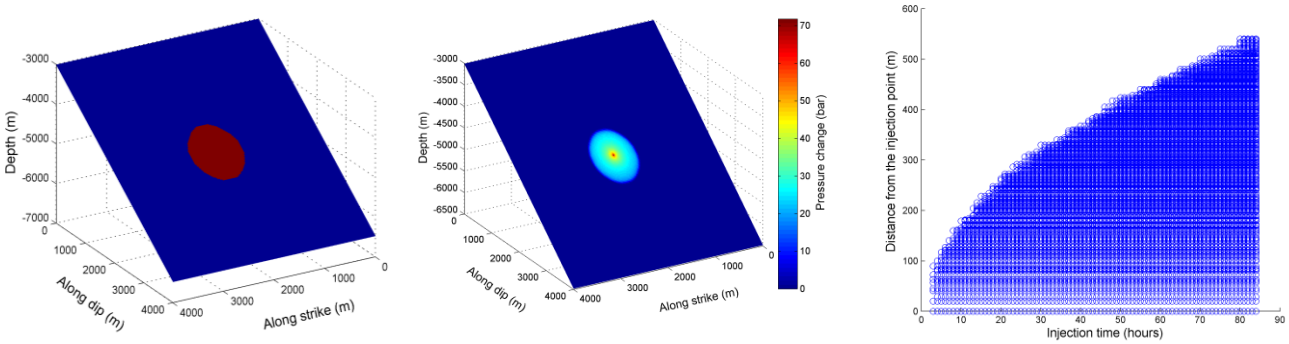

Figure 6 Reference scenario imposing a constant flow rate of 71.6 l/s at the injection well. a) Patches that failed at least once (red) after 70 hours of injection b) Pressure distribution (bar) on the fault plane after 70 hours of injection properties c) Distance-time plot of slip events.

The evolution of seismic moment with injection time is shown in Figure 7a. Given the injected volume and the shear modulus we can compute the maximum theoretical moment 2GΔV and the moment partitioning for this injection case, which is shown in Figure 7b. At the start of the injection the moment partitioning increases, but it becomes more and more constant with continuing injection. This trend is qualitatively consistent with the observations of the moment partitioning with time from cases shown in Figure 5b, where an increase in moment portioning is also often observed during the initial stage of injection, followed by a more or less constant moment portioning. The absolute value of the seismic moment is quite high for the modeling results, it is almost 10 times the moment predicted by 2GΔV.

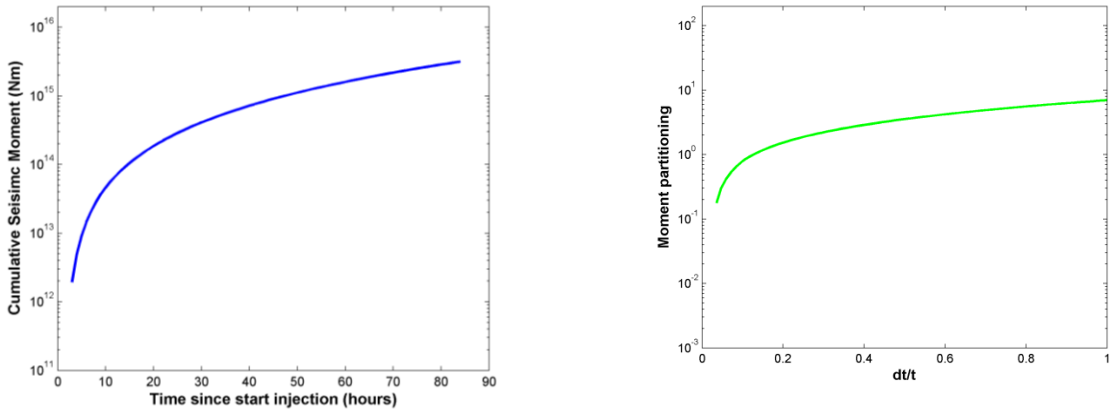

Figure 7 Evolution of cumulative seismic moment with injection time.

4.1 Effect of a highly stressed fault patch on slip event distribution and seismic moment

To investigate the effect of a highly stressed layer on the fault plane on the characteristics of the slip events we incorporated a square area with a lower coefficient of friction 300 m below the injection well. For the first 30 hours the slip events show the same evolution as the reference scenario. At that point the fluid front hits the critically stressed area, and the event activity increases, causing slip over the entire stressed area (Figure 8a). The required pressure increase to make the area slip is relatively low (Figure 8b). On the distance-time plot the point where the fluid front reaches the critically stressed area is indicated by a sudden increase in event distance at 30 hours (Figure 8c). The total event distance is larger than in the reference case, almost reaching 1000 m from the injection point. The moment partitioning with time shows a sudden jump as the fluid front hits the critically stressed region.

5 DISCUSSION

The magnitude versus volume data provide an update with more and more recent cases, and extends earlier data of increasing M_{max} with injection volume (Gerstenberger et al., 2013; Nicol et al., 2011). This increasing trend of M_{max} with volume is also in agreement with previous studies by McGarr (2002), who related the M_{max} to the lengthscale of the activity, and Klose (2013), who

related M_{max} to the mass change due to the activity. The moment partitioning (M_{0max} / GΔV) as proposed in this study provides a good tool to evaluate what fraction of the volume change is accommodated through seismic slip, and can be used to analyze the contribution of parameters that influence that fraction. In computing the theoretical maximum moment GΔV we have assumed a b-value of 1. Other b-values (in the range of 0.75 – 1.5) can be incorporated into the analysis and would influence the theoretical maximum moment (McGarr, 2014). For a b-value of 0.75 the GΔV would be a factor 2 with respect to a b-value of 1, for a b-value of 1.2 this would be a factor ½, and GΔV tends to zero for b-values approaching 1.5 as a result of the model setup. Thus, when the actual b-value would be different from 1 it could influence the results shown in Figure 3b somewhat by shifting the GΔV by a factor of 0.5 – 2, but it would not influence the general trends significantly. The general trends are also not sensitive to variations in the shear modulus.

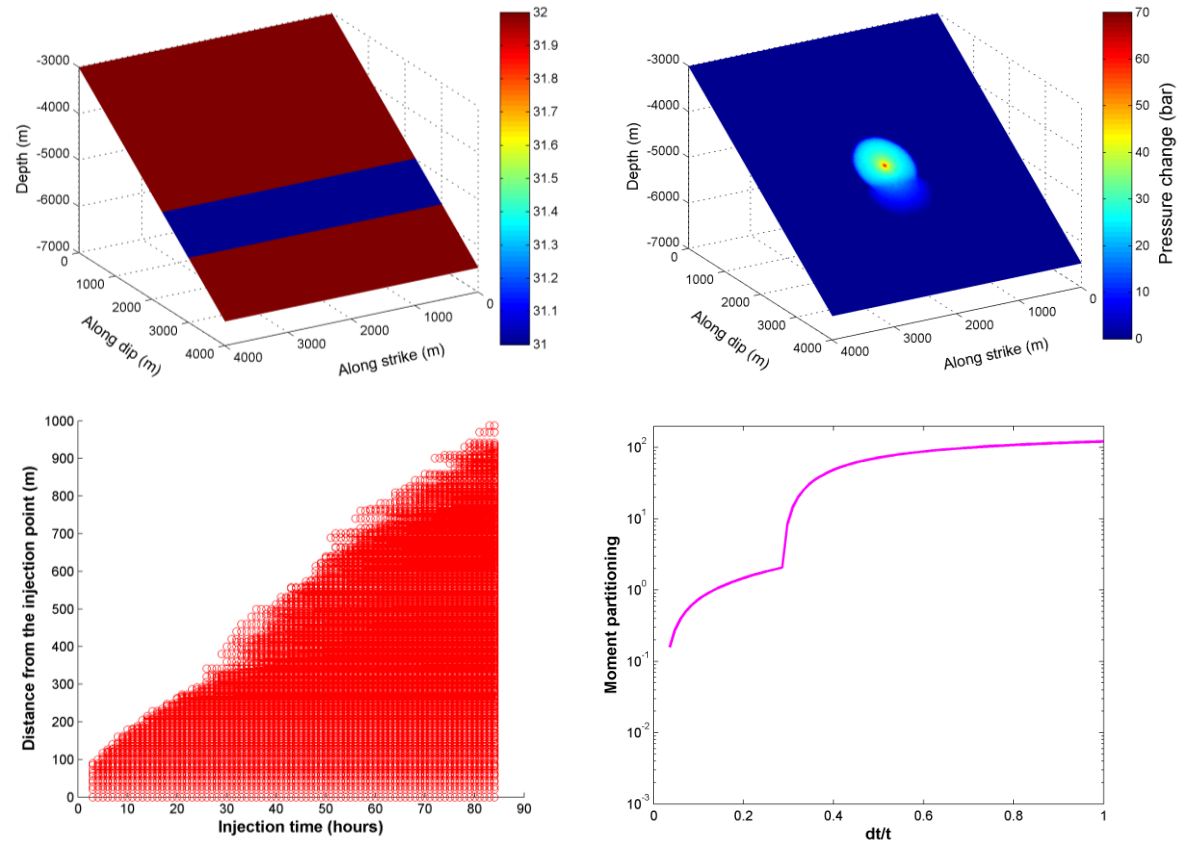

Figure 8 Initial distribution of friction angle on the fault plane. the blue area is very close to failure (friction angle 31°) top right) Distribution of pore pressure increase after 70 hours of injection bottom left) Distance time plot of slip events bottom right) moment partitioning as a function of injection time

We also observed that the moment partitioning was in some cases larger than 1, suggesting a major contribution of tectonic stress to the seismicity. In section 2.1 we discussed how the background state of stress was incorporated, namely through the assumption that faults are ½ a stress drop away from failure. However, if seismicity occurs primarily on critically stressed faults (i.e. very close to failure, much less than ½ a stress drop), formula (1) may underestimate the cumulative moment, because of the relatively large contribution of the pre-existing strain energy or tectonic stress. This is also termed 'triggered' form of seismicity: a very small stress change that gives a relatively large seismic response. The occurrence of this type of seismicity poses a large problem and is hard to avoid, since the stress changes required for triggering are so small. The relationship of the high moment partitioning cases with faults emphasizes the need for detailed seismic studies and stress analysis to avoid large, critically stressed, permeable fault structures.

We investigated a number of parameters influencing the moment partitioning, including the depth and the background seismicity. Relatively high moment fractions (>0.1) were observed for earthquakes occurring at depths of >3 km. With depth the differential stresses increase, and often more competent rocks exist at depth which sustain the larger stresses, which when released can create larger magnitude events and thus a larger partitioning factor. An increase in microseismic magnitudes with depth during hydraulic fracturing was also observed in shale plays in the US (Warpinski, 2012). For natural seismicity the b-value was observed to decrease with depth, also indicating a relatively large number of large magnitude earthquakes (Gerstenberger et al., 2001). For a number of waste water injection experiments it was observed that the large magnitude events actually occurred in the crystalline basement, below the layer targeted for injection. Crystalline rock masses are often found to be critically stressed, such as for example in Soultz-sous-Forêts and Basel. No correlation was observed for the moment partitioning and the regional seismic hazard, indicated by the PGA. Some of the largest moment fractions actually were observed in the aseismic intraplate area of the US. The PGA may be more an indicator of tectonic loading rate than of the state of stress. Intraplate loading rates are much slower, causing a much lower seismicity rate, but faults may still be under a critical state of stress.

The moment partitioning with relative injection time showed an initial increase, and then became more or less constant. The constant moment partitioning is consistent with the constant behavior of the seismogenic index Σ with injection time (Dinske & Shapiro, 2013). Comparing the equations for moment partitioning and the seismogenic index show that Σ is proportional to the moment fraction as $10^{-\Sigma}$. However, occasionally we observe sudden jumps in moment partitioning. This could indicate the reactivation of a larger critically stressed structure, and will be further analyzed using the numerical modelling results.

5.1 Applicability of the block-spring model to injection induced seismicity

We model injection induced seismicity on a single planar surface. In reality the injected fluids will not just percolate into a single planar surface, but stimulate a much larger connected fracture network. During injection experiments however often the microseismic events are often observed to line up along a linear structure, indicative of the reactivation of a larger scale fault structure oriented favorably in the stress field (eg. Charléty et al., 2007; Häring et al., 2008). These characteristics of the seismicity can be reproduced to a first order by models simulating seismicity on a single fault plane (Baisch et al., 2010; Wassing et al., in press). Variations in fault plane orientation may be included in the model by translating them into variations of frictional strength, with a lower strength for more favorably oriented fault patches and a higher strength for less well oriented fault patches. A major advantage of the block-spring model is that it runs very fast and provides for easy adaptation of the code.

The actual physics controlling slip on the fault patches and stress transfer is in the current model approximated through a prescribed stress drop and a prescribed transfer of a percentage of this stress drop to neighboring patches (Figure 2b). Since only the neighboring patches are affected, stress transfer attenuates very quickly and stress to patches further away is very limited. This causes the slipping area to be highly dependent on the pressure and the pressure gradient. This is evident from the model results, which show a strong confinement of the slipped patches to the area affected by the fluid front. Future research aims at incorporating more realistic friction laws and stress transfer in the model. Still, to a first order the current model results may be used to simulate characteristics of injection induced seismicity.

5.2 Comparison of modeling results and observations

To a first order the modeling results reproduce the evolution of seismic moment and moment partitioning observed in the injection cases analyzed in section 5. The modeled moment partitioning shows an initial increase and then becomes almost constant, similar to what was observed. The absolute values of moment partitioning are quite high and even exceed 1. In the model, there is no leak-off of fluids into the matrix or other fracture networks, so the pressure increase will be completely transferred to the fault cells. Also the fault is already near the failure equilibrium. As we discussed earlier, in the theoretical maximum moment $2G\Delta V$ it is assumed fault are on average half a stress drop away from failure. Whereas in nature this may be more applicable since the distribution of fault orientations is more distributed, in this case we have a single fault orientation which is very close to failure, and it is not surprising the moment partitioning is so high.

Including a more critically stressed area on the fault can produce a sudden jump in moment partitioning, similar to what was for example observed for the KTB injection or the Rocky Mountain Arsenal injection. The heterogeneous distribution of fault criticality may thus play a significant role in how the shear slip evolves with time. Other properties are also expected to influence the moment fraction and will be investigated in more detail in future research. By considering the response of the moment fraction to injection and fault parameters, numerical modeling may give valuable insights in what controls the moment partitioning.

6 CONCLUSIONS

In this research we have investigated the seismic response to fluid injection for a variety of cases. The main conclusions are:

- Magnitudes increase with volume
- Moment partitioning (ratio between observed seismic moment and theoretical moment induced by the injection) is mostly far less than 1. However, in a few cases, the moment fraction exceeds 1, indicating the contribution of a large tectonic event. These events often involve diffusion of fluid into a large fault structure, nucleating the large event at significant distance away from the injection point.
- Large moment fractions are observed to occur at significant depth (>4 km) for the cases investigated in our study. No influence of the regional seismic activity on moment partitioning was observed.
- The moment partitioning as a function of injection time shows an increase during the early 10-20% of injection and then levels off. In some cases however, a sudden increase in moment partitioning was observed.
- Numerical modeling of injection induced seismicity using a block-spring model is able to reproduce to a first order the observed evolution of moment partitioning with time.
- Applying a heterogeneous criticality on the modeled fault caused sudden changes in moment partitioning, similar to what was observed in some of the injection cases.
- The block-spring model can give valuable insights in the controls on moment partitioning and what controls how much of the strain induced by the injected fluid

REFERENCES

Baisch, S., Vörös, R., Rothert, E., Stang, H., Jung, R., & Schellschmidt, R.: A numerical model for fluid injection induced seismicity at Soultz-sous-Forêts, *International Journal of Rock Mechanics & Mining Sciences,* **47,** (2010) ,405.

Bendall, B., Hogarth, R., Holl, H., McMahon, A., Larking, A., & Reid, P.: Australian Experiences in EGS Permeability Enhancement – A Review of 3 Case Studies, *Thirty-Ninth Workshop on Geothermal Reservoir Engineering Stanford University, Stanford, California, February 24-26,* (2014).

Bommer, J. J., Oates, S., Cepeda, J. M., Lindholm, C., Bird, J., Torres, R., . . . Rivas, J.: Control of hazard due to seismicity induced by a hot fractured rock geothermal project, *Eng.Geol.,* **83,** (2006) ,287.

Charléty, J., Cuenot, N., Dorbath, L., Dorbath, C., Haessler, H., & Frogneux, M.: Large earthquakes during hydraulic stimulations at the geothermal site of Soultz-sous-Forêts, *International Journal of Rock Mechanics & Mining Sciences,* **44,** (2007) ,1091.

Cuenot, N., Dorbath, C., & Dorbath, L.: Analysis of the Microseismicity Induced by Fluid Injections at the EGS Site of Soultz-sous-Forêts (Alsace, France): Implications for the Characterization of the Geothermal Reservoir Properties, *Pure Appl.Geophys.,* **165,** (2008) ,797.

Deichmann, N., & Ernst, J.: Earthquake focal mechanisms of the induced seismicity in 2006 and 2007 below Basel (Switzerland), *Swiss Journal of Geoscience,* **102,** (2009) ,457.

Dinske, C., & Shapiro, S.: Seismotectonic state of reservoirs inferred from magnitude distributions of fluid-induced seismicity, *J.Seismol.,* **17,** (2013) ,13-25.

Dorbath, L., Cuenot, N., Genter, A., & Frogneux, M.: Seismic response of the fractured and faulted granite of Soultz-sous-Forêts (France) to 5 km deep massive water injections, *Geophysical Journal International,* **2003,** (2009) ,2004.

Eshelby, J. D.: The determination of the elastic field of an ellipsoidal inclusion, and related problems, *Proceedings of the Royal Society of London.Series A, Mathematical and Physical Sciences,* **241,** (1957) ,376-396.

Evans, K. F., Zappone, A., Kraft, T., Deichmann, N., & Moia, F.: A survey of the induced seismic responses to fluid injection in geothermal and CO2 reservoirs in Europe, *Geothermics,* **41,** (2012) ,30-54.

Fehler, M. C.: Stress Control of Seismicity Patterns Observed During Hydraulic Fracturing Experiments at the Fenton Hill Hot Dry Rock Geothermal Energy Site, New Mexico, *Int.J.Rock Mech.Min.Sci.,* **26,** (1989) ,211.

Gerstenberger, M., Nicol, A., Bromley, C., Carne, R., Chardot, L., Ellis, S., . . . Viskovic, P. (2013). Induced seismicity and its implications for CO2 storage risk.*Report No. RPT12-4001IEAGHG.*

Gerstenberger, M., Wiemer, S., & Giardini, D.: A systematic test of the hypothesis that the b value varies with depth in California, *Geophys.Res.Lett.,* **28,** (2001) ,57.

Giardini, D., GrÃ¼nthal, G., Shedlock, K. M., & Zhang, P.: The GSHAP Global Seismic Hazard Map, *Annals of Geophysics; Vol 42, No 6 (1999),* (1999)

Hanks, T. C., & Kanamori, H.: A Moment Magnitude Scale, *Journal of Geophysical Research,* **84,** (1979)

Häring, M. O., Schanz, U., Ladner, F., & Dyer, B. C.: Characterisation of the Basel 1 enhanced geothermal system, *Geothermics,* **37,** (2008) ,469.

Healy, J. H., Krivoy, H. L., Lane, M. P., Major, M., Jackson, W. H., & Van Schaack, J. H. (1966). Geophysical and geological investigations relating to earthquakes in the Denver area, Colorado.*Open File ReportU.S. Geological Survey.*

Jost, M. L., Büfelberg, T., Jost, O., & Harjes, H. -.: Source Parameters of Injection-Induced Microearthquakes at 9 km Depth at the KTB Deep Drilling Site, Germany, *Bulletin of the Seismological Society of America,* **88,** (1998) ,815.

Klose, C.: Mechanical and statistical evidence of the causality of human-made mass shifts on the Earth's upper crust and the occurrence of earthquakes, *J.Seismol.,* **17,** (2013) ,109-135.

Majer, E. L., Baria, R., Stark, M., Oates, S., Bommer, J., Smith, B., & Asanuma, H.: Induced seismicity associated with Enhanced Geothermal Systems, *Geothermics,* **36,** (2007) ,185.

Maxwell, S. C., Shemeta, J. E., Campbell, E., & Quirk, D. J.: Microseismic Deformation Rate Monitoring, *SPE Annual Technical Conference and Exhibition, 21-24 September, Denver, Colorado, USA,*

McGarr, A. (2002). Case histories of induced and triggered seismicity. In W. H. K. Lee, H. Kanamori, P. C. Jennings & C. Kisslinger (Eds.), *International handbook of earthquake and engineering seismology* (81A ed., pp. 647)

McGarr, A.: Maximum magnitude earthquakes induced by fluid injection, *Journal of Geophysical Research: Solid Earth,* (2014)

Moeck, I., Kwiatek, G., & Zimmermann, G.: Slip tendency analysis, fault reactivation potential and induced seismicity in a deep geothermal reservoir, *J.Struct.Geol.,* **31,** (2009) ,1174.

Nicol, A., Carne, R., Gerstenberger, M., & Christophersen, A.: Induced seismicity and its implications for CO2 storage risk, *Energy Procedia,* **4,** (2011) ,3699-3706.

Ohtake, M.: Seismic activity induced by water injection at Matsushiro, Japan, *Journal of Physics of the Earth,* **22,** (1974) ,163 - 176.

Rutledge, J. T., Phillips, W. S., & Mayerhofer, M. J.: Faulting Induced by Forced Fluid Injection and Fluid Flow Forced by Faulting: An Interpretation of Hydraulic-Fracture Microseismicity, Carthage Cotton Valley Gas Field, Texas, *Bulletin of the Seismological Society of America,* **94,** (2004) ,1817.

Shapiro, S., Krüger, O., Dinske, C., & Langenbruch, C.: Magnitudes of induced earthquakes and geometric scales of fluid-stimulated rock volumes, *Geophysics,* **76,** (2011) ,WC55-WC63.

Shapiro, S. A., Dinske, C., Langenbruch, C., & Wenzel, F.: Seismogenic index and magnitude probability of earthquakes induced during reservoir fluid stimulations, *The Leading Edge,* (2010) ,304.

Warpinski, N. R.: Measurements of hydraulic-fracture-induced seismicity in gas shales, *SPE Production and Operations,* (2012) ,240.

Wassing, B. B. T., van Wees, J. D., & Fokker, P. A.: Coupled continuum modeling of fracture reactivation and induced seismicity during enhanced geothermal operations, *Geothermics,* **xx,** (in press)

Table 2 Summary of data included in the statistical analysis. act = activity, with 2RC being secondary recovery, EGS = Enhanced Geothermal System, HF = hydraulic fracturing, DRI = fluid losses during drilling, EXP =injection experiment and WWI = waste water injection. PI signifies whether the maximum magnitude $_{Mmax}$ occurred post-injection (Y) or not (N). The d is the depth of the operation, dmmax is the hypocenter depth. The injected volume at the moment of Mmax (vmmax) is given in ^{m3}. PGA is the Peak Ground Acceleration in m^{s-2} with a 10% chance of being exceeded in 50 years.

site	country	act	mmax	pi	rock	d	dmmax	vmmax	pga
Cogdell Canyon Reef	USA	2RC	4.7	Y	Carbonate	2.1	3.0	4.2E+07	0.12
Eagle Field (Fort St. John)	CAN	2RC	4.3	Y	Carbonates & Sandstones	1.9		1.4E+06	0.31
Falls City Oil Field	USA	2RC	3.6	Y				1.0E+06	0.21
Rangely	USA	2RC	3.4	N	Sandstone	2.2		3.0E+07	0.62
Renqiu Oil Field well 845	CHN	2RC	4.5	Y	Carbonate	3.5	3.0	8.5E+04	0.84
Romashkino	RUS	2RC	4	N	Carbonates & Sandstones	1.7		1.5E+08	0.16
Shengli Field (Shandong)	CHN	2RC	2.4	N				6.4E+04	1.11
Swan Hills, Snipe Lake oil field	CAN	2RC	5.1	N	Carbonate	2.6	9.0	2.0E+07	0.11
St Gallen	SWZ	DRI	3.3	Y	Carbonate	4.5	4.5	6.5E+02	0.92
Basel 1	SWZ	EGS	3.4	N	Granite	4.6	4.6	1.2E+04	1.47
Berlin TR8A	SLV	EGS	4.4	N	Volcaniclastic	2.5	2.5	1.3E+05	3.29
Cooper basin Habanero-1 Main stimulation	AUS	EGS	3.7	N	Granite	4.3		8.0E+03	0.61
Cooper basin Habanero-1 Restimulation	AUS	EGS	3.0	N	Granite	4.3		3.0E+03	0.61
Gross Schoenebeck	DEU	EGS	-1.1	N	Volcaniclastic	4.1	4.0	1.3E+04	0.18
Hijiori HDR-1 1992	JPN	EGS	0.3	N	Granodiorite	2.2	2.1	2.1E+03	2.78
Hijiori HDR-1 1995	JPN	EGS	0.6	N	Granodiorite	2.2	1.6	1.1E+04	2.78
Hijiori SKG-2 1988	JPN	EGS	-0.5	N	Granodiorite	1.8	1.8	1.8E+03	2.78
Latera Deep Injection in Well L2	ITA	EGS	2.9	Y	Carbonate	2.7		2.0E+04	1.89
Latera Injection in Well L1 Test 2	ITA	EGS	0.5	N	Carbonate	1.7		5.4E+03	1.89
Latera Injection in Well L1 Test 3	ITA	EGS	0.5	N	Carbonate	1.7		5.0E+03	1.89
Latera Injection in Well L1 Test1	ITA	EGS	0.5	N	Carbonate	1.7		3.0E+03	1.89
Latera Injection in Well L6	ITA	EGS	0.8	N	Carbonate	1.7		2.7E+03	1.89
Ogachi OGC-1 1991	JPN	EGS	2.0	N	Granodiorite	1.0		1.0E+04	2.62
Ogachi OGC-1 1992	JPN	EGS	-1.0	N	Granodiorite	0.7		5.5E+03	2.62
Paralana 2 Inj period 1 & 2	AUS	EGS	2.5	N	Granite	3.7	4.0	9.3E+04	0.77
Paralana 2 Minifrac test	AUS	EGS	1.4	N	Granite	3.7	3.7	9.3E+04	0.77
Soultz-sous-Forets GPK2	FRA	EGS	2.5	Y	Granite	4.6	4.5	2.3E+04	0.76
Soultz-sous-Forets GPK3	FRA	EGS	2.9	Y	Granite	4.6	4.1	3.7E+04	0.76
Soultz-sous-Forets GPK4	FRA	EGS	2.3	Y	Granite	4.6	5.2	9.3E+03	0.76
Soultz-sous-Forets GPK4 2005 stimulation	FRA	EGS	2.7	N	Granite	4.6	4.8	8.0E+03	0.76

Torre Alfina Injection Borehole RA1	ITA	EGS	3.0	N	Carbonate	1.7		4.5E+03	2.02
KTB 1994 stimulation	DEU	EXP	1.2	N	Crystalline	9.1	8.6	1.0E+02	0.52
KTB 2000 stimulation	DEU	EXP	1.1	N	Crystalline	5.5		8.6E+01	0.52
Nojima Fault Zone, 2d injection	JPN	EXP	1.0	N		1.8		2.1E+02	3.20
Barnett Shale, North, single frac	USA	HF	-1.5	N	Shale	1.7		1.2E+03	0.13
Blackpool Stage 2	GBR	HF	2.3	Y	Shale	2.7		2.3E+03	0.46
Blackpool Stage 4	GBR	HF	1.5	N	Shale	2.5		1.7E+03	0.46
Cold Lake water injection experiment 1995 Phase 2	CAN	HF	-1.1	N	Shale	0.2	0.2	3.2E+02	0.10
Cotton Valley, Carthage Gas Field	USA	HF	-1.5	N	Sands & Shales	2.8		1.0E+03	0.20
Eola Field Picket Unit B Well 4-18 stage 2	USA	HF	2.9	Y	Sandstone	3.0	3.1	9.4E+03	0.38
Horn River basin d-1-D Microseismic monitoring	CAN	HF	3.1	N	Shale	2.8		5.0E+03	0.42
Horn River basin Etsho area C-034	CAN	HF	3.8	N	Shale	2.7		6.0E+04	0.42
Ashtabula (OH)	USA	WWI	4.3	Y	Sandstone	1.8	3.7	3.4E+05	0.25
Dallas Fort Worth (TX)	USA	WWI	3.3	N	Carbonate	4.2		3.7E+05	0.16
Guy & Greenbrier	USA	WWI	4.7	N	Carbonates & Sandstones	3.3	6.0	1.3E+05	0.66
Huangjiachang gasfield, Zigong, Sichuan	CHN	WWI	4.4	N	Carbonate	2.5	5.3	1.0E+04	2.18
Matsushiro	JPN	WWI	2.5	N	Crystalline	1.8	6.5	2.9E+03	2.22
Matsushiro	JPN	WWI	2.8	Y	Crystalline	1.8	7.0	3.2E+01	2.22
Paradox Valley	USA	WWI	4.3	N	Carbonate	4.5		3.2E+06	0.49
Perry, Cleveland (OH), Calhio #1 well	USA	WWI	4.9	N	Carbonates & Sandstones	1.9	5.0	1.4E+06	0.26
Prague (OK)	USA	WWI	5.7	N	Carbonate	1.1	4.0	1.6E+05	0.35
Rocky Mountain Arsenal, Denver (CO)	USA	WWI	4.8	Y	Crystalline	3.8	3.0	6.2E+05	0.31
Rongchang Luo-4 & Luo-2 wells	CHN	WWI	5.2	N		2.7	13.0	1.0E+06	0.60
Trinidad	USA	WWI	5.3	Y	Sands & Shales	1.8	4.0	4.9E+06	0.42
Youngstown, Northstar 1 (OH)	USA	WWI	3.9	Y	Various	2.7	3.7	7.8E+04	0.23